Journal of Alloys and Compounds 509 (2011) 5667–5671

Contents lists available at ScienceDirect

Journal of Alloys and Compounds

journal homepage: www.elsevier.com/locate/jallcom

Carbon nanotube–chitosan composite electrodes for electrochemical removal of Cu(II) ions

Yankun Zhan, Likun Pan*, Chunyang Nie, Haibo Li, Zhuo Sun

Engineering Research Center for Nanophotonics & Advanced Instrument, Ministry of Education, Department of Physics, East China Normal University, Shanghai 200062, China

ARTICLE INFO

Article history:
Received 20 November 2010
Received in revised form 19 February 2011
Accepted 21 February 2011
Available online 1 March 2011

Keywords:
Carbon nanotube
Chitosan
Cu(II) ion
Composite electrode
Electrochemical removal

ABSTRACT

Carbon nanotube–chitosan (CNT–CS) composite electrodes are prepared by firstly reacting oxidized CNT with thionyl chloride and then covalently grafting CS onto the surface of CNT. The electrochemical removal of Cu^{2+} ions by CNT–CS composite electrodes is investigated. The results show that CNT–CS Exhibits 85% Cu^{2+} removal ratio, 25% higher than that of pristine CNT, due to its lower zeta potential, higher surface area, more hydrophilic surface and more binding sites.

1. Introduction

Cupric ions (Cu^{2+}) commonly exist in the waste water of several industries such as acid mine, acidic corrosion of pipes and electroplating waste. The presence of excessive amounts of Cu^{2+} in drinking water may lead to accumulation in the liver and cause gastrointestinal problems [1]. Therefore, it is significantly important to remove Cu^{2+} from water. Various approaches have been adopted to remove Cu^{2+} including precipitation, electrochemical treatment, chemical reduction, solvent extraction, ion exchange and adsorption [2–4]. However, the application of these processes is often limited because of technical or economic constraint. Electrosorption, defined as adsorption on the surface of charged electrode by applying potential or current, has attracted a great interest due to its low energy consumption and environmental friendliness [5–9]. Electrosorption has been successfully used to remove Cu^{2+} and the difficulty of electrode regeneration due to the electrodeposition reaction on the electrode surface when applied voltage is above some value can be solved by combining reverse voltage and short circuit [10,11].

As a key component of electrosorption device, the development and optimization of electrode materials should be the focus. Carbon nanotube (CNT) has been proved to be a competitive and promising electrode material for adsorption or electrosorption due to its large surface area, high mechanical strength, remarkable electrical conductivity and high stability [12–18]. However, the hydrophobicity of CNT limits its application in electrosorption. Currently the functionalization of CNT with nontoxic and hydrophilic polymers promises to be one of the most successful methods to improve the hydrophilicity of CNT. These polymers can bring a hydrophilic surface on CNT and create more sorption sites. One of the common polymers that is used for the modification of CNT is chitosan (CS) [19,20]. As an inexpensive, widely used and nontoxic polysaccharide biopolymer, CS displays excellent film-forming ability, high hydrophilicity, and good biocompatibility [21–24]. Because CS has abundant amino ($-NH_2$) and/or hydroxy (–OH) functional groups which serve as coordination sites and exhibit a high specificity toward metal ions [25–27], CS has been integrated with CNT to form CNT–CS composites to effectively remove Cu^{2+} from aqueous solutions by adsorption method [28] or to determine Cu^{2+} by anodic stripping voltammetry [29]. Unfortunately, so far the exploration on the application CNT–CS composite materials for electrosorption is hardly reported.

In this work, we fabricate CNT–CS composite materials by covalent functionalization of CNT with CS and study their electrochemical removal behavior in Cu^{2+} solution. An applied voltage of 1.2 V is used in this work. Due to intrinsic resistance of the electrodes which consume some voltage, electrodeposition does not happen remarkably and electrosorption is mainly responsible for the removal of Cu^{2+} ions. However, considering a small contribution from Cu electrodeposition during dominant electrosorption process, the term "electrochemical removal" [30] is used here.

* Corresponding author. Tel.: +86 21 62234132; fax: +86 21 62234321.
E-mail address: lkpan@phy.ecnu.edu.cn (L. Pan).

0925-8388/$ – see front matter © 2011 Elsevier B.V. All rights reserved.
doi:10.1016/j.jallcom.2011.02.118

2. Experimental

2.1. Preparation

CNT–CS composite materials were synthesized from multi-walled CNT (>95% purity, Shenzhen Nano-tech Port Co. Ltd., China) via a modified Zhu's method [31]. Briefly, 2 g CNT was added in 100 mL HNO_3 solution and refluxed for 7 h at 140 °C. After being filtrated, washed to neutral and dried overnight, the oxidized CNT was subsequently reacted with 40 mL 5 wt% thionyl chloride ($SOCl_2$) in toluene for 5 h at 70 °C and purified through the Soxlet extraction. Then the treated CNT was mixed with 0.5 g CS in 50 mL aqueous solution with 2 wt% acetic acid (CS dissolves easily in acid solution) and then stirred for 24 h.

Finally the mixture was dropped onto the graphite paper with a thickness of 1 mm (Qingdao Huatai lubricant sealing S&T Co. Ltd), dried at 100 °C for 5 h. After being washed by large amounts of deionized water and dried under vacuum to remove the residue reagents, the mass of formed CNT–CS film was 0.7 g and the content of CS in the composite was about 25%. Two CNT–CS electrodes were assembled in holders. The effective area of each electrode was 64 cm^2 (8 cm × 8 cm) and the distance between the electrodes was 2 mm. Two pristine CNT electrodes (each 0.7 g) were also fabricated and assembled for comparison.

2.2. Characterization

The surface morphology and structure were characterized by field emission scanning electron microscopy (FESEM, JEOL-4700), transmission electron microscope (TEM, JEM-2100), Fourier transform infrared spectroscopy (FTIR, Nexus 670) and X-ray Photoelectron Spectroscopy (XPS) using a Kratos AXIS spectrometer with monochromatic Al Kα (1486.71 eV) X-ray radiation, respectively. The contents of C, H, S, and N were quantitatively analyzed by a CHNS/O elemental analyzer (VARIOEL3, Elementar). The pH value of the solution was adjusted between 2 and 10 by adding HCl or NaOH and the pH of the point of zero charge was measured using a Zeta Meter (JS94J, Powereach). The contact angle of water on the surface of electrode was measured by contact angle goniometer (JC2000D, Powereach) using digital micrographs of deionized water droplets. The specific surface area and pore size distribution were determined by surface analyzer (O2108-KR-1, Quantachrome) using N_2 as adsorbate at 77 K.

2.3. Electrochemical removal experiments

Electrochemical removal experiments were conducted in a continuously recycling system including a removal unit cell, as described in our previous works [11,32,33]. The analytical pure cupric chloride ($CuCl_2$) was used for the aqueous solutions. In each experiment, the solution was continuously pumped from a peristaltic pump into the cell and the effluent returned to the unit cell. The solution temperature was kept at 295 K and a flow rate around 40 mL min^{-1} was applied. The electrochemical removal was performed by a DC power supply at a constant voltage (1.2 V) and the variation of Cu^{2+} concentration was measured by a conductivity meter (DDS-308, Precision & Scientific Instrument) in situ. The relationship between conductivity and concentration was obtained according to a calibration table made prior to the experiments. Fig. 1 shows the relationship between solution conductivity z (μS cm^{-1}) and Cu^{2+} concentration C (mg L^{-1}, measured using Solar M6 atomic absorption spectroscopy). It can be seen that the relationship follows the linear plot based on the following equation:

$$C = 0.632 \times z - 1.90 (R^2 = 0.997) \quad (1)$$

The regression coefficient R^2 of Eq. (1) is 0.997. The amount of Cu^{2+} removal q_e (mg g^{-1}) was calculated from the following equation:

$$q_e = (C_0 - C_e)V/m \quad (2)$$

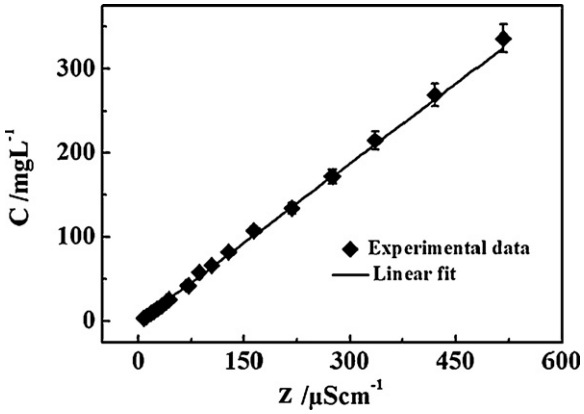

Fig. 1. The relationship between solution conductivity z and Cu^{2+} concentration C.

where C_0 (mg L^{-1}) and C_e (mg L^{-1}) are the initial and equilibrium concentration of Cu^{2+}, respectively. V (L) is the volume of the solution and m (g) is the mass of CNT or CNT–CS electrodes.

3. Results and discussion

Fig. 2(a) and (b) shows the FESEM images of CNT and CNT–CS. It can be observed that CNT has a snake-like shape. While CNT–CS displays a more compact surface in which wire-like CNT is dispersed in the CS matrix. The inset of Fig. 2(a) and (b) displays the TEM images of CNT and CNT–CS. The length of CNT is found to be reduced from original 4 μm to 1 μm in CNT–CS composite, which should be due to the treatment of HNO_3 [34]. The shorter CNT may contribute to the enhanced specific surface area, as observed in Table 1. The measured BET surface areas and the average pore diameter is changed from 44.5 m^2 g^{-1} and 21.9 nm for CNT to 52.7 m^2 g^{-1} and 8.3 nm for CNT–CS, which offers a higher accessible surface area and will be beneficial to Cu^{2+} removal performance [35,36].

Fig. 3 shows the FTIR spectra of CNT and CNT–CS. Compared with CNT, CNT–CS exhibits several new characteristic groups [31,37–39]. C=O stretching vibrations (1850 cm^{-1}) and O–H bend-

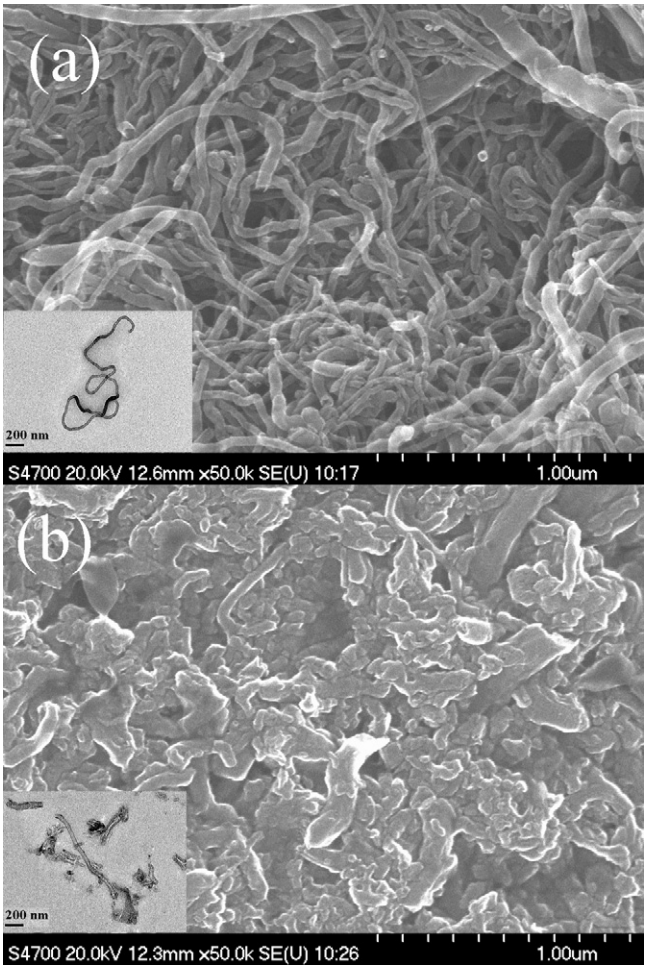

Fig. 2. FESEM images of (a) CNT and (b) CNT–CS. Insets are their TEM images.

Table 1
Surface characteristic of CNT and CNT–CS.

Sample	Surface area (m^2 g^{-1})	Average pore diameter (nm)	Pore volume (cm^3 g^{-1})	pH_{pzc}
CNT	44.5	21.9	10.2	5.30
CNT–CS	52.7	8.3	12.1	4.38

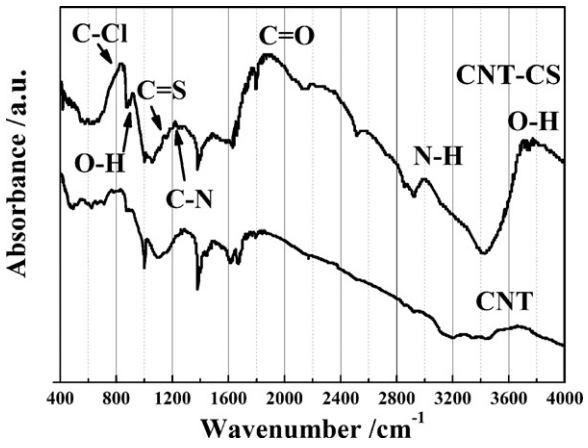

Fig. 3. FTIR spectra of CNT and CNT–CS.

Table 2
Elemental compositions of CNT and CNT–CS.

	C (%)	H (%)	N (%)	S (%)
CNT	98.28	<0.3	<0.3	<0.5
CNT–CS	69.78	3.14	3.17	0.76

ing vibrations (920 cm^{-1}) confirm the existence of –COOH group. C–Cl (832.7 cm^{-1}) and C=S (1132.7 cm^{-1}) stretching bands are ascribed to the successful modification of $SOCl_2$. These acidic functional groups can create more defect sites for ion sorption and facilitate the connection between CNT and CS. The decoration of CNT by CS is validated by the existence of C–N stretching vibrations (1219.2 cm^{-1}), N–H (3007.7 cm^{-1}) and O–H stretching bands (3800 cm^{-1}). Furthermore, elemental composition analysis of CNT and CNT–CS by CHNS/O elemental analyzer (Table 2) shows that N, S and H contents substantially increase in CNT–CS, which further confirms that CS has been successfully grafted onto CNT.

Fig. 4 plots the zeta potential of CNT and CNT–CS. As the pH value increases, the zeta potential decreases and the values of CNT–CS are more negative than those of CNT. Their pH values of point of zero charge (pH_{pzc}), as shown in Table 1, are 5.30 and 4.38, respectively. The more negative pH_{pzc} of CNT–CS, also reported by other studies [40], indicates that acidic functional groups are present in CNT–CS, which will favor the electrostatic adsorption of Cu^{2+}. Fig. 5 shows the photographic images of water droplet onto the surface of CNT and CNT–CS. The measured contact angle decreases from 86° for CNT to 56.5° for CNT–CS indicating that surface hydrophilicity is improved by the introduction of the functional groups [41]. The

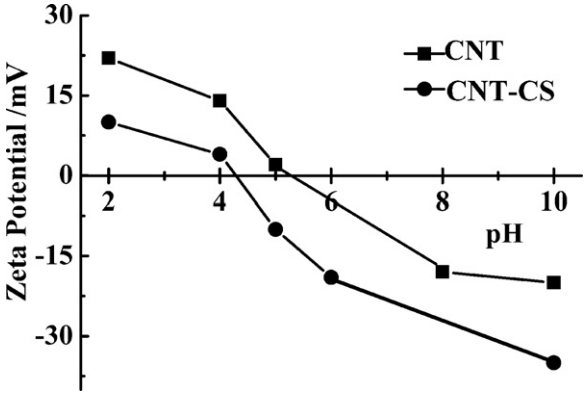

Fig. 4. Zeta potential of CNT and CNT–CS as a function of pH value.

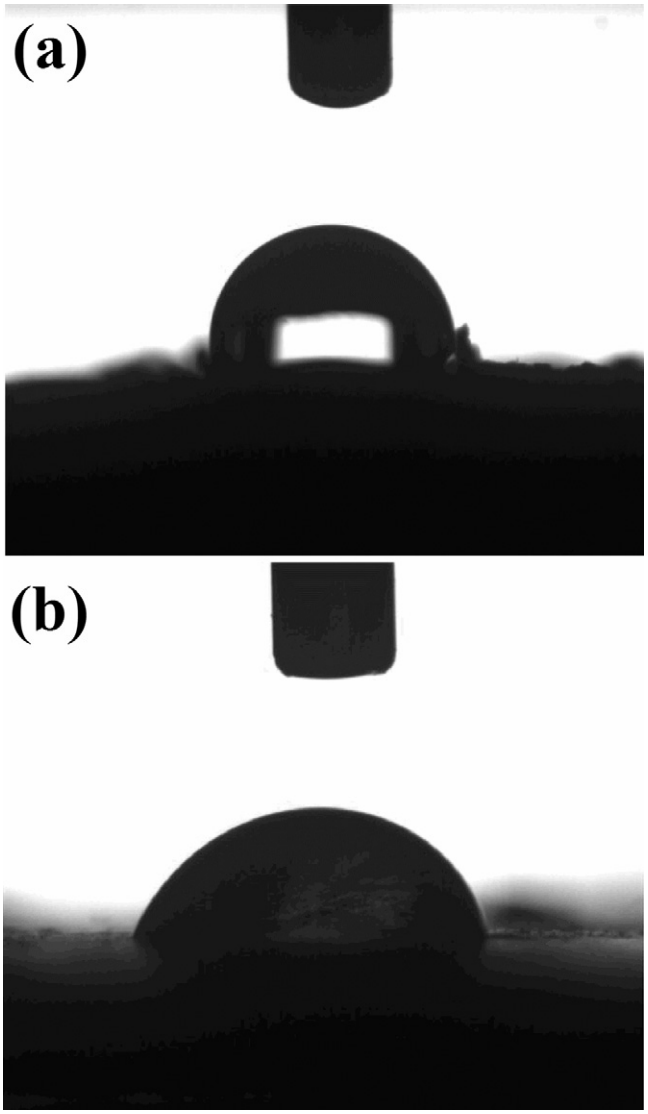

Fig. 5. Photographic images of water droplets on the surface of (a) CNT and (b) CNT–CS.

hydrophilic surface benefits Cu^{2+} adsorption. As known, Cu^{2+} exists in aqueous solution mostly in the form of hydrated ions, functional groups on the pore wall can affect the behavior of confined water molecules leading to amazed water adsorption [42] and meanwhile increase adsorption of hydrated Cu^{2+}.

Fig. 6(a) shows the variation of solution conductivity with time during the electrochemical removal of Cu^{2+} by CNT and CNT–CS. The initial conductivity of $CuCl_2$ solution is 50 μS/cm. When the voltage is not applied, no obvious physical adsorption is found for both CNT and CNT–CS. Once the voltage is imposed, ions are driven onto the electrodes and the conductivity decreases and reaches equilibrium after about 240 min. It shows that Cu^{2+} removal is significantly improved under the electric field and total Cu^{2+} removal is mainly contributed by electrochemical removal. Compared with CNT, CNT–CS presents 85% Cu^{2+} removal ratio, 25% higher than that of CNT (60%). The result states clearly that CNT–CS exhibits better electro-assisted Cu^{2+} removal properties.

The electrochemical removal rate constants of Cu^{2+} onto CNT and CNT–CS can be obtained by fitting the experimental data using model equations including pseudo-first-order kinetics and pseudo-second-order kinetics. Pseudo-first-order kinetics model is found

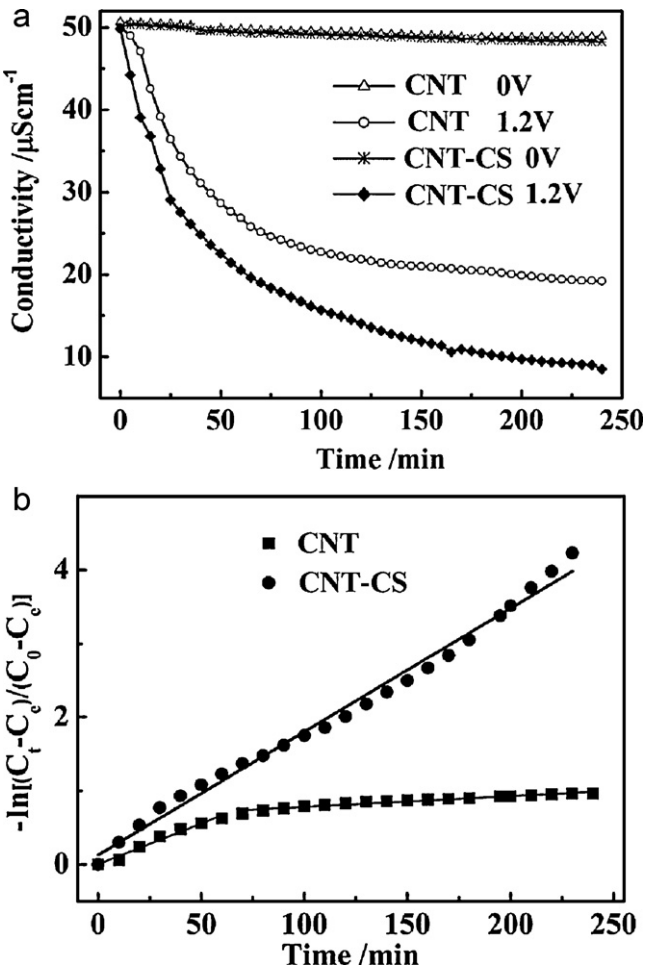

Fig. 6. (a) Variation of solution conductivity with time and (b) linear plot of the pseudo-first-order kinetic equation for electrochemical removal of Cu^{2+} by CNT and CNT–CS.

to describe the experimental data better than pseudo-second-order kinetics model in this work and can be formulated as [43]:

$$\ln\left[\frac{C_t - C_e}{C_0 - C_e}\right] = -kt \quad (3)$$

where k (min^{-1}) is the rate constant, C_0, C_e and C_t ($mg\,L^{-1}$) are initial concentration, equilibrium concentration and the concentration at time t (min), respectively. The kinetics parameters can be obtained by fitting the experimental data using least square method, as shown in Fig. 6(b) and Table 3. The experimental data of CNT–CS is found to be in agreement with the pseudo-first-order rate law very well and the rate constant is 0.017 min^{-1}, while CNT exhibits two linear segments with the rate constants of 0.011 min^{-1} (0–70 min) and 0.002 min^{-1} (70–240 min), respectively. The very small rate constant in second segment should be ascribed to removal saturation effect after 70 min. As compared with CNT, CNT–CS exhibits higher kinetics rate constant, which is beneficial to the Cu^{2+} removal.

Table 3
Parameters of pseudo-first-order kinetics for the electrochemical removal of Cu^{2+} at 1.2 V.

	k (min^{-1})	Coefficient of determination (R^2)
CNT (0–70 min)	0.011	0.971
CNT (70–240 min)	0.002	0.944
CNT–CS	0.017	0.995

As mentioned above, an applied voltage of 1.2 V is beyond the potential window of Cu^{2+} electrolysis and Cu will be electrodeposited on the surface of CNT–CS. To characterize the contribution from Cu electrodeposition to total removal of Cu^{2+}, surface elemental composition of CNT–CS after the electrochemical removal of Cu^{2+} is analyzed by XPS spectra, as shown in Fig. 7. Before XPS measurement, CNT–CS electrode is washed by deionized water to get rid of the residue Cu^{2+}. Therefore, Cu on the surface of CNT–CS almost exists in the form of solid. It can be observed that the atomic ratio of Cu is only 0.29%, very small in all elements. This confirms that electrodeposition does not happen remarkably due to intrinsic resistance of the electrodes which consume some voltage and electrosorption is mainly responsible for the removal of Cu^{2+} ions. It should be noticed that the electrodeposition reaction will affect electrode regeneration. Fortunately, this problem has been solved by combining reverse voltage and short circuit [10,11]. The long-term performance of the CNT–CS electrode is very stable and decay in Cu^{2+} removal has not been obviously observed after 30 charge–discharge cycles.

To further compare Cu^{2+} removal behavior of CNT and CNT–CS, the batch experiments with different initial conductivities ranging from 30 to 400 μS/cm were carried out. Langmuir isotherm (Eq. (4)) and Freundlich isotherm (Eq. (5)) are used to fit the experimental data [32].

$$q_e = \frac{q_m K_L C_e}{1 + K_L C_e} \quad (4)$$

$$q_e = K_F C_e^{1/n} \quad (5)$$

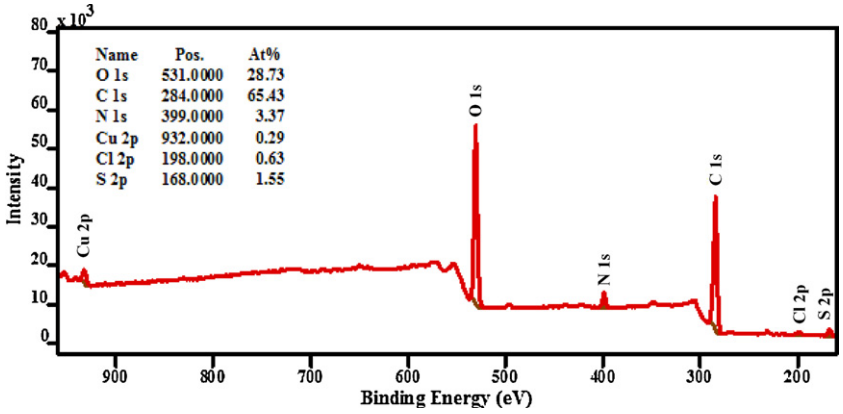

Fig. 7. Surface elemental composition of CNT–CS electrode after the electrochemical removal of Cu^{2+} by XPS measurement.

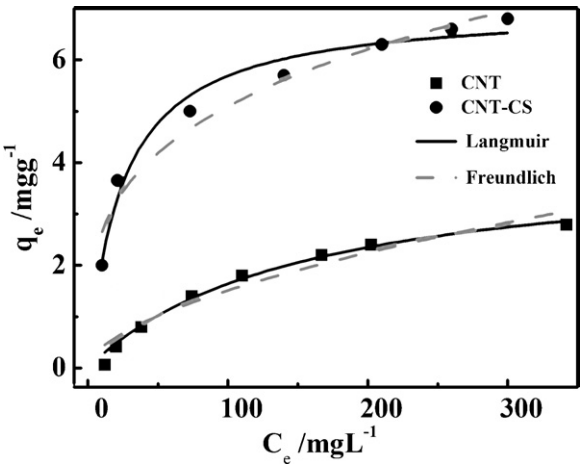

Fig. 8. Equilibrium isotherms of CNT and CNT–CS in $CuCl_2$ solution.

Table 4
Parameters determined from isotherms of CNT and CNT–CS in $CuCl_2$ solution.

Isotherm	Model equation	Parameter	CNT	CNT–CS
Langmuir	$q_e = \frac{q_m K_L C_e}{1+K_L C_e}$	q_m	3.96	7.2
		K_L	0.007	0.035
		R^2	0.993	0.991
Freundlich	$q_e = K_F C_e^{1/n}$	K_F	0.166	1.379
		$1/n$	0.495	0.284
		R^2	0.955	0.953

where q_e (mg g^{-1}) is the amount of removed $CuCl_2$ and q_m (mg g^{-1}) is the maximum removal capacity corresponding to complete monolayer coverage. K_L and K_F are Langmuir constant that relates to the affinity of binding sites and Freundlich constant, respectively. Fig. 8 shows the fitting results and the removal capacities increase with the concentration and then reach a plateau. The parameters of Langmuir and Freundlich models for Cu^{2+} removal on CNT and CNT–CS are listed in Table 4. From the regression coefficient R^2, Langmuir isotherm fits the experimental data of both CNT and CNT–CS better than Freundlich isotherm, suggesting that for modeling purposes, Cu^{2+} monolayer coverage and equal activation energy during removal process can be assumed. According to Langmuir model, after CS grafting, K_L increases from 0.007 to 0.035 indicating more affinity of the binding sites on CNT–CS. Moreover, the maximum Cu^{2+} removal capacities are 3.96 and 7.2 mg g^{-1} for CNT and CNT–CS, respectively. It shows that Cu^{2+} removal has been effectively enhanced after the decoration of CS on the CNT.

4. Conclusions

In this work, we develop CNT–CS composite electrode material for electrochemical removal of Cu^{2+}. The experimental results show that (1) as compared with pristine CNT, CNT–CS exhibits lower zeta potential, higher surface area, more hydrophilic surface and more binding sites, which are beneficial to Cu^{2+} removal; (2) the isotherm studies of CNT and CNT–CS electrodes show that both of them follow Langmuir adsorption, suggesting that Cu^{2+} monolayer coverage and equal activation energy during electrochemical removal process can be assumed; (3) CNT–CS Exhibits 25% higher Cu^{2+} removal ratio with a higher removal rate constant than that of CNT and (4) CNT–CS may be potential candidate as electrode materials for Cu^{2+} removal.

Acknowledgement

This work was supported by Special Project for Nanotechnology of Shanghai (no. 1052nm02700).

References

[1] E. Orozco-Guareno, F. Santiago-Gutierrez, J.L. Moran-Quiroz, S.L. Hernandez-Olmos, V. Soto, W. de la Cruz, R. Manriquez, S. Gomez-Salazar, J. Colloid Interf. Sci. 349 (2010) 583.
[2] Y. Chen, B. Pan, H. Li, W. Zhang, L. Lv, J. Wu, Environ. Sci. Technol. 44 (2010) 3508.
[3] B. Kizilkaya, A.A. Tekinay, Y. Dilgin, Desalination 264 (2010) 37.
[4] Y.M. Hao, M. Chen, Z.B. Hu, J. Hazard. Mater. 184 (2010) 392.
[5] Y.J. Kim, J.H. Choi, Water Res. 44 (2010) 990.
[6] S. Nadakatti, M. Tendulkar, M. Kadam, Desalination 268 (2011) 182.
[7] M. Wang, Z.H. Huang, L. Wang, M.X. Wang, F. Kang, H. Hou, New J. Chem. 34 (2010) 1843.
[8] R. Zhao, P.M. Biesheuvel, H. Miedema, H. Bruning, A. van der Wal, J. Phys. Chem. Lett. 1 (2010) 205.
[9] L.M. Chang, X.Y. Duan, W. Liu, Desalination 270 (2011) 285.
[10] H. Oda, Carbon 41 (2003) 1037.
[11] Y.K. Zhan, H.B. Li, L.K. Pan, Y.P. Zhang, Y.W. Chen, Z. Sun, Water Sci. Technol. 61 (2010) 1427.
[12] M.A. Salam, M. Mokhtar, S.N. Basahel, S.A. Al-Thabaiti, A.Y. Obaid, J. Alloys Compd. 500 (2010) 87.
[13] J. Zhang, L. Gao, J. Alloys Compd. 505 (2010) 604.
[14] M.H.A. Kudus, H.M. Akil, H. Mohamad, L.F. Loon, J. Alloys Compd. 509 (2011) 2784.
[15] B. Scheibe, E. Borowiak-Palen, R.J. Kalenczuk, J. Alloys Compd. 500 (2010) 117.
[16] X.S. Liu, F. Hu, D.R. Zhu, D.N. Jia, P.P. Wang, Z. Ruan, C.H. Cheng, J. Alloys Compd. 509 (2011) 2829.
[17] Y.C. Su, C.A. Chen, Y.M. Chen, Y.S. Huang, K.Y. Lee, K.K. Tiong, J. Alloys Compd. 509 (2011) 2011.
[18] Y.C. Bai, W.D. Zhang, C.H. Chen, J.Q. Zhang, J. Alloys Compd. 509 (2011) 1029.
[19] I. Olivas-Armendariz, P. Garcia-Casillas, R. Martinez-Sanchez, A. Martinez-Villafane, C.A. Martinez-Perez, J. Alloys Compd. 495 (2010) 592.
[20] H. Yang, R. Yuan, Y. Chai, Y. Zhuo, Colloids Surf. B 82 (2011) 463.
[21] H. Liu, F. Yang, Y. Zheng, J. Kang, J. Qu, J.P. Chen, Water Res. 45 (2011) 145.
[22] B. Feng, R.Y. Hong, Y.J. Wu, G.H. Liu, L.H. Zhong, Y. Zheng, J.M. Ding, D.G. Wei, J. Alloys Compd. 473 (2009) 356.
[23] D.L. Zhao, X.X. Wang, X.W. Zeng, Q.S. Xia, J.T. Tang, J. Alloys Compd. 477 (2009) 739.
[24] G.Y. Li, Y.R. Jiang, K.L. Huang, P. Ding, J. Chen, J. Alloys Compd. 466 (2008) 451.
[25] A. Ghaee, M. Shariaty-Niassar, J. Barzin, T. Matsuura, Chem. Eng. J. 165 (2010) 46.
[26] F.Y. Shih, K.Z. Fung, J. Alloys Compd. 430 (2007) 320.
[27] S. Verbych, M. Bryk, G. Chornokur, B. Fuhr, Sep. Sci. Technol. 40 (2005) 1749.
[28] M.A. Salam, M.S.I. Makki, M.Y.A. Abdelaal, J. Alloys Compd. 509 (2011) 2582.
[29] B.C. Janegitz, L.H. Marcolino-Junior, S.P. Campana-Fillho, R.C. Faria, O. Fatibello-Filho, Sens. Actuators B 142 (2009) 260.
[30] Y. Bouhadana, E. Avraham, A. Soffer, D. Aurbach, AIChE J. 56 (2010) 779.
[31] J.Z. Zhu, B.L. Deng, J. Yang, D.C. Gang, Carbon 47 (2009) 2014.
[32] H.B. Li, T. Lu, L.K. Pan, Y.P. Zhang, Z. Sun, J. Mater. Chem. 19 (2009) 6773.
[33] H.B. Li, Y. Gao, L.K. Pan, Y.P. Zhang, Y.W. Chen, Z. Sun, Water Res. 42 (2008) 4923.
[34] X.B. Li, X.Y. Jiang, New Carbon Mater. 25 (2010) 237.
[35] Y. Han, X. Quan, S. Chen, S. Wang, Y. Zhang, Electrochim. Acta 52 (2007) 3075.
[36] Y. Gao, L.K. Pan, H.B. Li, Y.P. Zhang, Z.J. Zhang, Y.W. Chen, Z. Sun, Thin Solid Films 517 (2009) 1616.
[37] Y.H. Li, S.G. Wang, Z.K. Luan, J. Ding, C.L. Xua, D.H. Wu, Carbon 41 (2003) 1057.
[38] A.A. El-Hendawy, J. Anal. Appl. Pyrolysis 75 (2006) 159.
[39] C.S. Lu, H.S. Chiu, Chem. Eng. Sci. 61 (2006) 1138.
[40] B. Kannamba, K.L. Reddy, B.V. Apparao, J. Hazard. Mater. 175 (2010) 939.
[41] Y.H. Li, Y. Zhu, Y. Zhao, D. Wu, Z. Luan, Diamond Relat. Mater. 15 (2006) 90.
[42] A. Striolo, P.K. Naicker, A.A. Chialvo, P.T. Cummings, K.E. Gubbins, Adsorption 11 (2005) 397.
[43] S. Lagergren, Handlingar 24 (1898) 1.